NJC

PAPER

View Article Online
View Journal

Cite this: DOI: 10.1039/c8nj04493g

The effects of molecular structure and functional group of a rodlike Schiff base mesogen on blue phase stabilization in a chiral system†

Chiung-Cheng Huang, *[a] Yu-Chang Huang,[a] Wei-Cheng Hsieh,[a] Yen-Jung Chen,[a] Shi-Kai Jiang,[a] Bo-Hao Chen,[bc] I.-Jui Hsu*[bd] and Jey-Jau Lee[c]

Received 6th September 2018,
Accepted 17th December 2018

DOI: 10.1039/c8nj04493g

rsc.li/njc

Two types of racemic rodlike Schiff base mesogens with –C=N– (type **I**) and –N=C– (type **III**) linkages were prepared. These mesogens possessed either difluoro substitutions at the inner-core position of the phenyl ring or hydroxy group to form intramolecular hydrogen bonding with an ester or/and imine linkage. When the appropriate concentration of chiral additive is doped into them, the incorporation of two fluoro substituents is more useful for blue phase (BP) stabilization than that of a hydroxy group near the ester linkage in Schiff base mesogens. BPI and BPII can be identified by reflectance spectra and polarized optical microscope images. BPII emerges easily on cooling when the appropriate chiral dopant **ISO(6OBA)$_2$** or chiral dopant **S811** is doped into the Schiff base mesogen having only a hydroxy group near the ester linkage. Interestingly, BPI can be observed when 10–15 wt% **ISO(6OBA)$_2$** was doped into the difluoro substituted Schiff base mesogen **III** during a heating process. The experimental and molecular modeling results indicate that most of the difluorinated Schiff base mesogens with larger dipole moments exhibit wider BP ranges than their corresponding non-fluorinated homologues under the same chirality condition. In addition, wide BPs can be induced for racemic rodlike Schiff base mesogens **I** in the chiral system and this is easier than that for racemic rodlike Schiff base mesogens **III**. In Schiff base mesogens **I**, the dipole moment is dominant for BP stabilization. However, the fluorine substituent effect is the main factor in Schiff base mesogens **III**.

1. Introduction

Blue phase liquid crystals (BPLCs) have drawn significant research interest because they possess excellent physical properties such as great potential in wide viewing angle,[1,2] fast response[3–6] low energy consumption in liquid crystal displays,[7] self-organized optical isotropy,[8,9] a short response time down to the sub-millisecond range,[10] and tunability of soft photonic devices.[11,12] Consequently, they have the potential to develop next-generation display technology, photonics and electro-optic device applications. BPs are fluid three-dimensional periodic structures between an isotropic and a chiral nematic phase. BPLCs are considered to form a helically double twisted cylinder (DTC) structure and can be classified into BPI (body center cubic), BPII (simple cubic) and BPIII (amorphous) in accordance with the stacking of DTCs in a cubic lattice.[13] However, the defect (disclination) of the fluid three-dimensional periodic structure in a cubic lattice makes BP unstable and this results in a narrow temperature range. Thus, the practical applicability of a display device based on BPLCs is limited. Recently, a significant number of researchers have been developing many methodologies to overcome these disadvantages in temperature stability. Synthetic chemists can design novel BP mesogens with optically pure groups and high chirality, such as bent-core,[14,15] T-shaped,[16–19] U-shaped[20] and (−)-menthol-based biphenyl molecules, which possess a high twisting power (HTP) to form a helix.[21] Other LC research groups generally utilize convenient blending techniques. Kikuchi *et al.* first introduced polymers into the disclination in the cubic lattice to broaden the BP range which is more than 60 K.[22] Subsequently, the properties and applications of polymer-stabilized BPLCs have been systematically investigated and demonstrated.[23] In addition, the disclination in cubic lattice BPCLs can also be stabilized by nanoparticles.[24] Besides polymer and nanoparticle stabilizations, Yang's group first developed self-assembled LC complexes by hydrogen bonding to induce wide BPLCs (23 K).[25] On the

---

[a] *Department of Chemical Engineering, Tatung University, Taipei 104, Taiwan. E-mail: chchhuang@ttu.edu.tw; Tel: +886-2-77364681*
[b] *Department of Molecular Science and Engineering, National Taipei University of Technology, Taipei 106, Taiwan*
[c] *National Synchrotron Radiation Research Center, Hsinchu 300, Taiwan*
[d] *Research and Development Center for Smart Textile Technology, National Taipei University of Technology, Taipei 106, Taiwan. E-mail: ijuihsu@mail.ntut.edu.tw; Tel: +886-2-27712171 # 2420*

† Electronic supplementary information (ESI) available. See DOI: 10.1039/c8nj04493g

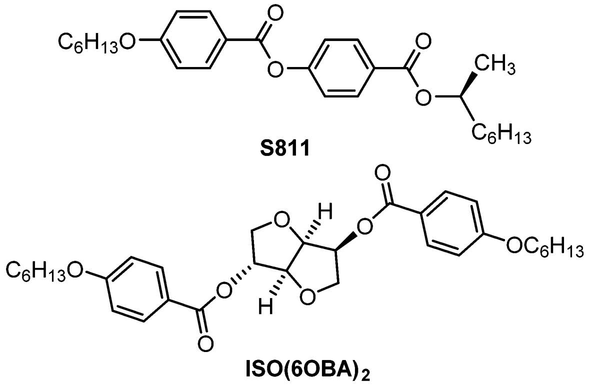

Fig. 1 Chemical structures of chiral dopants **S811** and **ISO(6OBA)$_2$**.

other hand, Yang's group found that lateral fluoro substituents of the mesogen play crucial roles in broadening the BP temperature range.[26] Moreover, bent-core molecules with giant flexoelectricity, which were doped into chiral nematic LCs to increase the elastic constant K_{33} and improve the thermal stability, have been confirmed.[27–31] Furthermore, the photoresponsive bent-core molecule with azo linkage can be photoinduced to fill in the disclination in 3D cubic lattices and induce wider BP ranges.[32–36] Accordingly, these studies proposed that chirality, elasticity, flexoelectricity, lateral fluoro-substitution, and molecular biaxiality play important roles in BP stabilization.[16]

Imine or Schiff base (azomethine) as a linking group is widely utilized in many types of LC molecular structure. Its derivative, salicylaldimine[*N*-(2-hydroxy-4-alkoxybenzylidene) aniline], possesses the ability to coordinate metals to form metallomesogens as a result of the presence of the hydroxy group.[37] Recently, Schiff bases, such as ferrocene-based Schiff base metallomesogen,[38] chiral three-ring calamitic Schiff base mesogens,[39] unsymmetrical and symmetric Schiff base dimers[40,41] and photoresponsive bent-core molecules,[33] have also been widely applied in BPLCs. Some of these BPLCs exhibit wide BP ranges and are stable at room temperature. However, only a few simple rodlike Schiff base molecules were utilized to induce wide BPs. Recently, we induced an unprecedented wide BP temperature range (>30 K) by doping the chiral dopant **S811,** at *ca.* 35 wt%, into the racemic rodlike Schiff base mesogen with alkynyl linkage.[42,43] The BP temperature range can also be extended by adding 10 wt% **ISO(6OBA)$_2$** into the racemic rodlike Schiff base mesogen possessing ester linkage. We proposed that a larger super-cooling and viscosity effect from the hydroxy group near the imine linkage of a Schiff base mesogen could result in a broad BP temperature range. Nevertheless, the effects of molecular structure and functional group of the Schiff base mesogen on BP stabilization are still not established thoroughly. Therefore, in this work, two homologous series of rodlike Schiff base mesogens with –C=N– (type **I**) and –N=C– (type **III**) linkages were prepared (Fig. 1 and 2).

To the best of our knowledge, these Schiff base mesogens that possessed intramolecular hydrogen bonding *via* hydroxy groups with ester or imine linkages, and difluoro substitutions at the inner-core position of the phenyl ring have never been reported up to now. The mesomorphism and thermal behaviours of these Schiff base mesogens were investigated by X-ray diffraction (XRD), differential scanning calorimetry (DSC) and the characteristic texture of polarized optical microscopy (POM). Subsequently, we doped appropriate concentrations of chiral dopants **S811** and **ISO(6OBA)$_2$** into these Schiff base mesogens to investigate the effects of molecular structure and functional group of these rodlike Schiff base mesogens on BP stabilization in a chiral system.

2. Experimental

2.1. Spectroscopic analysis

The chemical structures of the target materials were identified by proton nuclear magnetic resonance (^{1}H NMR) spectroscopy using a Bruker Avance DRX 500 NMR spectrometer (Bruker Co., Karlsruhe, Germany). The purity of the final compounds was assessed by thin layer chromatography (TLC), and further confirmed by elemental analysis using a Heraeus Vario EL **III** analyzer (Elementar Analysenyteme GmbH Co., Hanau, Germany). Variable-temperature XRD experiments were performed at the wiggler beam-line BL17A at the National Synchrotron Radiation Research Center (NSRRC), Taiwan. The experimental wavelength is 1.3214 Å, and the sample was packed into a 0.5 mm capillary. A heat gun was equipped at this beamline and the temperature controller was programmable by a PC with a PID feedback system. The experimental XRD pattern was indexed by DICVOL program to obtain the crystal system and cell constants.[44–46]

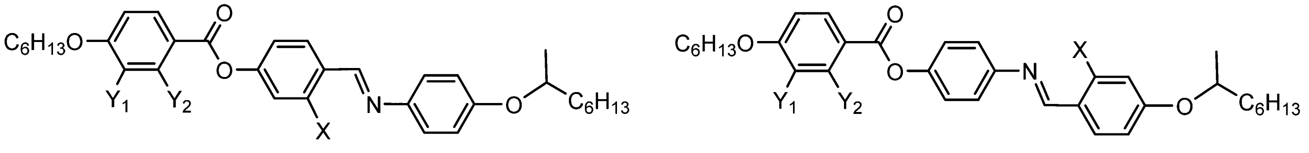

H-EI$_6$: X = H, Y_1 = H, Y_2 = H
H-EI$_6$-OH: X = H, Y_1 = H, Y_2 = OH
H-EI$_6$-F: X = H, Y_1 = F, Y_2 = F
OH-EI$_6$: X = OH, Y_1 = H, Y_2 = H
OH-EI$_6$-OH: X = OH, Y_1 = H, Y_2 = OH
OH-EI$_6$-F: X = OH, Y_1 = F, Y_2 = F

H-EIII$_6$: X = H, Y_1 = H, Y_2 = H
H-EIII$_6$-OH: X = H, Y_1 = H, Y_2 = OH
H-EIII$_6$-F: X = H, Y_1 = F, Y_2 = F
OH-EIII$_6$: X = OH, Y_1 = H, Y_2 = H
OH-EIII$_6$-OH: X = OH, Y_1 = H, Y_2 = OH
OH-EIII$_6$-F: X = OH, Y_1 = F, Y_2 = F

Fig. 2 Molecular structures of Schiff base mesogens.

2.2. Liquid-crystal and physical properties

The initial phase sequence and corresponding transition temperature of the compounds were determined by POM. Mesophases were principally identified by the microscopic texture of the materials sandwiched between two glass plates under a crossed polarizing microscope using a Nikon Microphoto-FXA optical microscope in conjunction with a hot stage controlled by a control processor. The phase transition temperatures and corresponding phase transition enthalpies of compounds were determined by DSC using a Perkin Elmer Diamond calorimeter under running rates of 3 °C min^{-1}. The Bragg reflection spectra of BPs were recorded with a USB2000 spectrometer in reflection mode, and the temperature of the samples was controlled accurately by the hot stage.

2.3. Preparation of materials

All of the starting materials were purchased from Sigma-Aldrich with purity greater than 99%. Thin layer chromatography was performed using TLC sheets coated with silica; spots were detected by UV irradiation. Silica gel (Merck silica gel 60, 63-200 mesh) was used for column chromatography. The organic solvents were dried and distilled before use. 4-(Hexyloxy)-2-hydroxybenzoic acid, 2,3-difluoro-4-(hexyloxy)benzoic acid and 4-(hexyloxy)benzoic acid were synthesized according to the literature.[47,48] Detailed synthetic procedures for the intermediates and target materials are described below. In addition, the molecular structures of the target products and the intermediates were confirmed by spectroscopic analysis and microanalytical data, as described in the ESI.†

Synthesis of A. To a solution of 4-(hexyloxy)-2-hydroxybenzoic acid or 2,3-difluoro-4-(hexyloxy)benzoic acid (15.2 mmol) and 4-hydroxybenzaldehyde or 2,4-dihydroxybenzaldehyde (10.1 mmol) in dichloromethane (10 ml), *N*,*N*′-dicyclohexylcarbodiimide (30.3 mmol) and 4-dimethylaminopyridine (1.1 mmol) were added in an ice bath. The solution mixture was stirred at room temperature for 2 days. Precipitates were removed by filtration. The solvent was removed and the obtained residue was purified by column chromatography over silica gel using EtOAc/hexane (1 : 4) as the eluent. The crude product was further purified by repeated recrystallization from methanol to give a white solid.

Synthesis of Schiff base mesogens (type I). A mixture of **A** (9.0 mmol) and 4-(1-methylheptoxy)aniline (9.0 mmol) in ethanol (10 mL) was refluxed for 4 h. After cooling to room temperature, a yellow precipitate was obtained and collected by filtration. The crude product was further purified by repeated recrystallization from ethanol to give a yellow powder in 50–60% yield.

Synthesis of compound B. It was synthesized by using the same synthetic method as that described for compound **A**. The crude product was further purified by repeated recrystallization from methanol to give a white solid in 55–60% yield.

Synthesis of compound C. To a solution of compound **B** (5.5 mmol) in dry ethyl acetate (10 mL), Pd/C (0.1 g, 1.1 mmol) was added and stirred under a hydrogen atmosphere (balloon) for 24 h (monitored by TLC). The reaction mixture was then filtered through a celite bed. The filtrate was concentrated under reduced pressure to give a yellow or white solid in 90–95% yield.

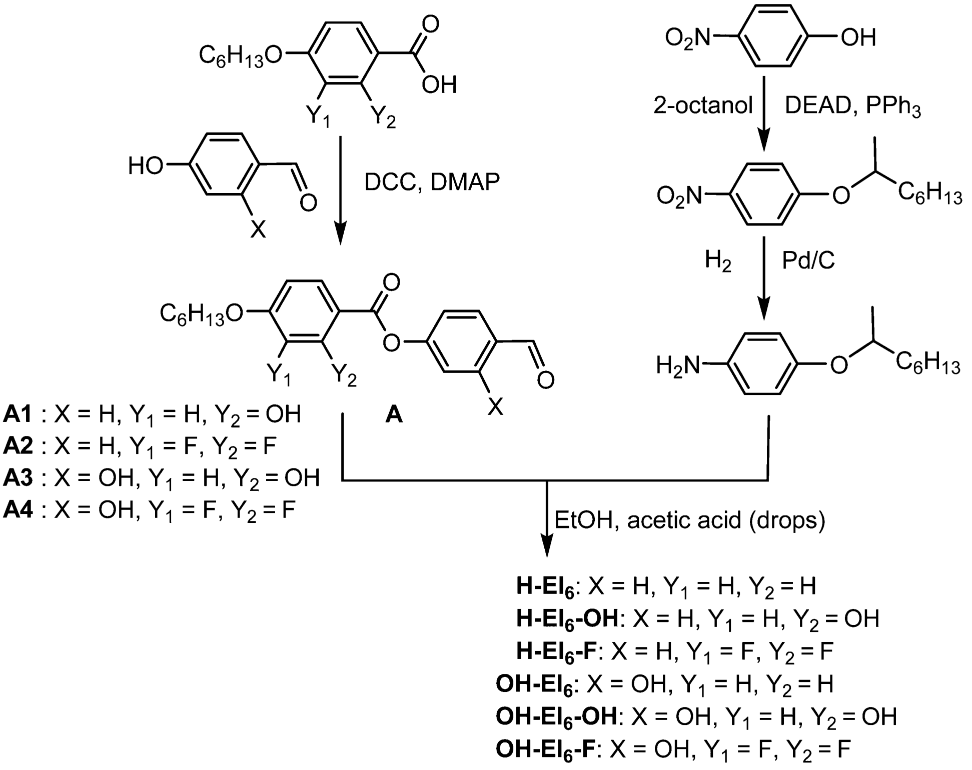

Scheme 1 Synthetic route of Schiff base mesogens of type I.

Synthesis of compound D. A solution of diisopropyl azodicarboxylate (7.2 mmol) and 4-hydroxybenzaldehyde or 2,4-dihydroxybenzaldehyde (7.2 mmol) in 10 mL of anhydrous THF was added drop by drop to a solution of triphenylphosphine (7.2 mmol) and 2-octanol (7.2 mmol) in 15 mL of anhydrous THF at room temperature with stirring for 24 h. After a work-up procedure, this product was isolated by column chromatography over silica gel using toluene as eluent. A colorless oil was obtained in 50–60% yield.

Synthesis of Schiff base mesogens (type III). A mixture of **C** (9.0 mmol) and **D** (9.0 mmol) in ethanol (10 mL) was refluxed for 4 h. After cooling to room temperature, a yellow precipitate was obtained and collected by filtration. The crude product was further purified by repeated recrystallization from ethanol to give a yellow or white powder in 50–60% yield.

Theoretical calculation. All density functional theory (DFT) calculations were performed in the Gaussian09 package.[49] The calculation strategy is based on our previous report.[42,43] The coordinates used for geometry optimization of all Schiff base compounds were initially built in the Avogadro program[50] then optimized by the long-range corrected hybrid functional CAM-B3LYP[51] in the G09 program. The basis set of 6-311G(d,p) was used to calculate the dipole moment and polarizability. In order to compare the dipole moment of all molecules, the origin was set at the center of the phenyl ring, and the *x*-axis is parallel with the longitudinal direction and *z*-axis is perpendicular to the phenyl plane. The molecular structures, dipole moments, and isosurface plots of the molecular orbitals were generated using GaussView5.0.[52]

3. Results and discussion

3.1. Synthesis and molecular structure characterization of rodlike Schiff base mesogen

The synthetic steps of ten rodlike Schiff base mesogens are shown in Schemes 1 and 2. At first, four compounds **A** were prepared by Steglich esterification reaction of 4-hydroxybenzaldehyde or 2,4-dihydroxybenzaldehyde with 4-(hexyloxy)-2-hydroxybenzoic acid or 2,3-difluoro-4-(hexyloxy)benzoic acid in the presence of dicyclohexylcarbodiimide (DCC) as a coupling reagent and 4-dimethylaminopyridine (DMAP) as a catalyst. Similarly, three compounds **B** could be obtained by Steglich esterification condition. Subsequently, these nitro materials were hydrogenated using hydrogen gas and Pd/C as a catalyst to obtain compound **C** with an amino group. Compounds **D** could be synthesized by Mitzunobu reaction. In the final step, compounds **A** were condensed with 4-(1-methylheptoxy)aniline in ethanol to obtain

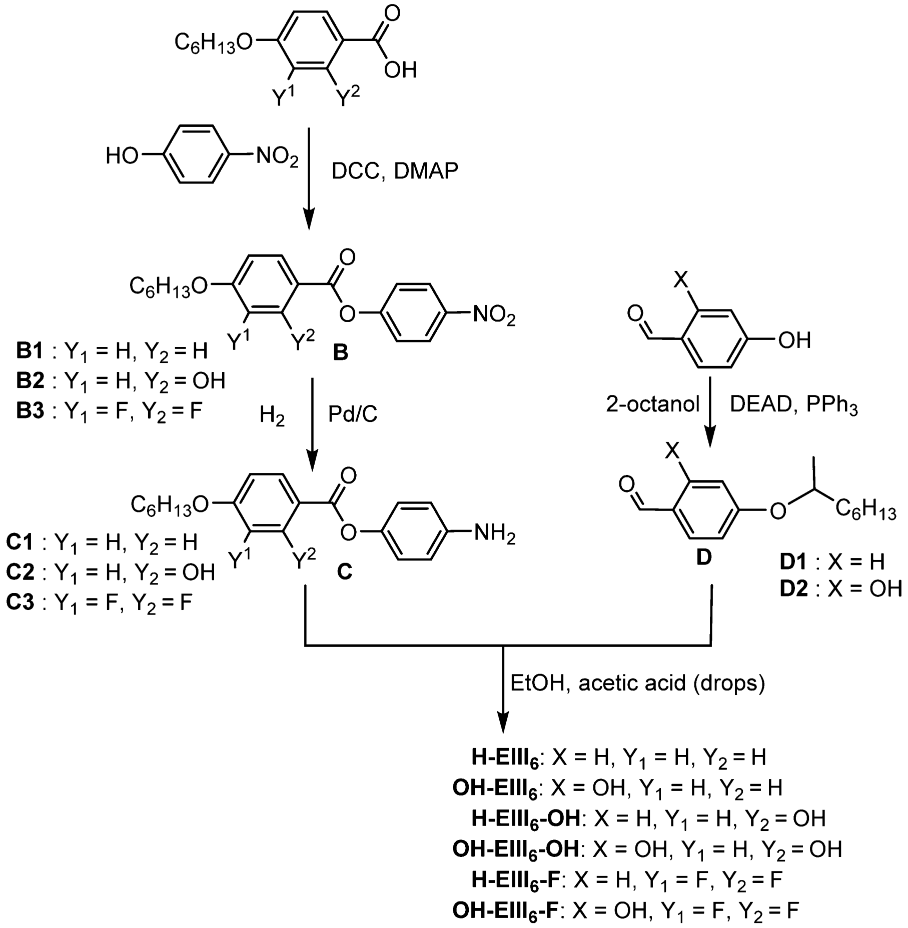

Scheme 2 Synthetic route of Schiff base mesogens of type **III**.

the targeted racemic rodlike Schiff base mesogens **I** with –C=N– linkage. Racemic rodlike Schiff base mesogens **III** with –N=C– linkage could be prepared from anilines **C** and aldehyde **D** by the same method. In the ^{1}H NMR spectra of Schiff base mesogens **OH-EI$_6$-OH** with two hydroxy groups, the chemical shift of the **–OH** hydrogen adjacent to the ester group appears at *ca.* 10.5 ppm and one characteristic peak in the range of 13–14 ppm indicates another proton that forms the intramolecular hydrogen bond with the imine linkage (Fig. S1a, ESI†). Similar chemical shifts can be observed in the ^{1}H NMR spectrum of **OH-EIII$_6$-OH** (Fig. S1b, ESI†). In addition, the existence of the intramolecular hydrogen bonding between the hydroxy group and ester linkage in these Schiff base mesogens can be confirmed by C=O with a lower frequency (*ca.* 1680 cm^{-1}) than the general ester group in the FT-IR spectra (Fig. S2, ESI†).

3.2. The phase transition behaviors of ten Schiff base mesogens

The phase transition temperatures and enthalpies of ten Schiff base mesogens shown in Table 1 were determined by DSC (Fig. S3, ESI†), POM (Fig. 3 and Fig. S4–S7, ESI†) and XRD (Fig. S8, ESI†). Most of these rodlike Schiff base mesogens exhibit nematic and smectic mesophoric behaviors. Notably, Schiff base mesogen **OH-EI$_6$-OH** possessing two hydroxy groups exhibits a wider interval of the nematic phase (83.6 K).

Fig. 3 shows its POM textures on cooling. The schlieren texture that can be observed at 103.3 °C indicates the appearance of a nematic phase. On further cooling to near room temperature (33.6 °C), the striated texture or transition bar appears, indicating the characteristic transition of nematic to smectic C phase. At room temperature, the schlieren texture of four brush singularities for the SmC phase can be observed. In addition, the incorporation of difluoro substitutions into the inner-core position of the phenyl ring or intramolecular hydrogen bonding *via* the hydroxy group with the ester results in the clearing point of the Schiff base mesogen declining. Furthermore, the Schiff base mesogen that possessed a hydroxy group near the ester linkage to form intramolecular hydrogen bonding exhibits a lower clearing point in comparison with its homologue that possessed intramolecular hydrogen bonding next to the imine linkage. On the other hand, the incorporation of intramolecular hydrogen bonding between the hydroxy group and ester linkage in the Schiff base mesogen could reduce the molecular interaction and stacking, which may result in the temperature range of the nematic phase increasing and that of the smectic phase decreasing for LC properties. However, two fluoro substituents protrude from the side of the mesogenic core to shorten the temperature range of the nematic phase and widen that of the smectic phase. Notably, only Schiff base mesogen **H-EIII$_6$-OH** shows enantiotropic nematic phases and no smectic mesomorphism, and is similar to biphenyl mesogens **CnOBiPhI-OH** possessing a hydroxy group near the ester linkage.[53]

3.3. Effect of the hydroxy group position and fluoro substituents on BP ranges

In accordance with previous reports,[42,43] BPs could emerge after 20.0 wt% chiral dopants **S811** or 5 wt% **ISO(6OBA)$_2$** are

Table 1 Phase transition temperature and corresponding transition enthalpies of Schiff base mesogens[a]

	Phase sequence[b] (°C, ΔH/kJ mol^{-1})	
Compounds	Cooling	Heating
H-EI$_6$-OH	Iso 109.9(2.40) N 34.8(0.83) SmC < 20 Cr	Cr 85.0(36.76) N 112.2(0.58) Iso
H-EI$_6$-F	Iso 94.8(0.24) N 76.4(0.62) SmC < 20 Cr	Cr 30.7(11.26) SmC 77.5(0.37) N 109.7(0.17) Iso
OH-EI$_6$-OH	Iso 111.6(0.56) N 33.0(0.36) SmC < 20 Cr	Cr 41.7(8.44) N 112.4(0.42) Iso
OH-EI$_6$-F	Iso 124.6(0.25) N 96.1(2.42) SmC < 20 Cr	Cr 65.8(22.36) SmC 95.3(0.77) N 121.8(0.53) Iso
H-EIII$_6$	Iso 126.1(0.59) N 58.5(1.15) SmC < 20 Cr	Cr 75.2(33.69) N 117.67(0.82) Iso
H-EIII$_6$-OH	Iso 96.0(0.74) N < 20 Cr	Cr 42.71(21.35) N 97.8(0.50) Iso
H-EIII$_6$-F	Iso 125.6(0.72) N 72.4(0.80) SmC < 20 Cr	Cr 69.3(22.90) N 124.0(0.70) Iso
OH-EIII$_6$	Iso 154.1(1.10) N 128.9(0.40) SmC < 20 Cr	Cr 65.8(26.63) SmC 129.7(0.48) N 154.7(1.14) Iso
OH-EIII$_6$-OH	Iso 104.6(0.43) N 73.3(0.24) SmC < 20 Cr	Cr < 20 SmC 66.7(0.30) N 103.9(0.59) Iso
OH-EIII$_6$-F	Iso 141.0(1.20) N 120.0(1.32) SmC 64.6(35.9) Cr	Cr 74.0(37.30) SmC 120.5(1.44) N 141.5(1.18) Iso

[a] Peak temperature in the DSC profiles obtained during the second heating and cooling cycles at a rate of 3 °C min^{-1}. [b] N = nematic; SmC = smectic C; Cr: crystal.

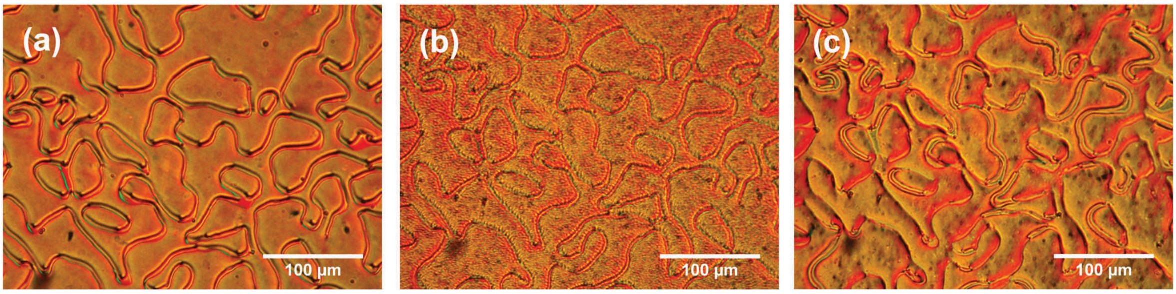

Fig. 3 Microphotographs for compound **OH-EI$_6$-OH**: (a) N texture at 103.3 °C; (b) N–SmC texture at 33.6 °C; (c) SmC texture at 30.0 °C.

added into the racemic rodlike Schiff base mesogens. And, we have demonstrated that the stabilization of blue phases for rodlike Schiff base mesogens in binary mixture systems is not correlated with HTP. Moreover, we also found that the hydroxy group in the molecular structures of rodlike Schiff bases dominated BP stabilization. As most of these rodlike Schiff base mesogens possess a hydroxy group, it is necessary to figure out the effect of the hydroxy group position of rodlike Schiff base mesogens on BP ranges in chiral systems. The phase transition temperatures of the binary mixtures were identified by POM during the cooling process at 0.2 °C·min^{-1}.

Fig. 4 shows the phase diagrams of rodlike Schiff base mesogens **I** doped with different concentrations (20–40 wt%) of chiral additive **S811**. With a hydroxy group at the inner-core phenyl ring to form intramolecular hydrogen bonding with the ester linkage, Schiff base mesogens **H-EI$_6$-OH** and **OH-EI$_6$-OH** exhibited a lower BP emerging temperature and narrower BP range in comparison with their homologues **H-EI$_6$** and **OH-EI$_6$** under the same chirality condition. However, with the incorporation of two fluoro substituents into the molecular structure, Schiff base mesogens **H-EI$_6$-F** and **OH-EI$_6$-F** exhibit a wide BP range (*ca.* 17–18 K) in chiral systems with **S811** even though their BP emerging

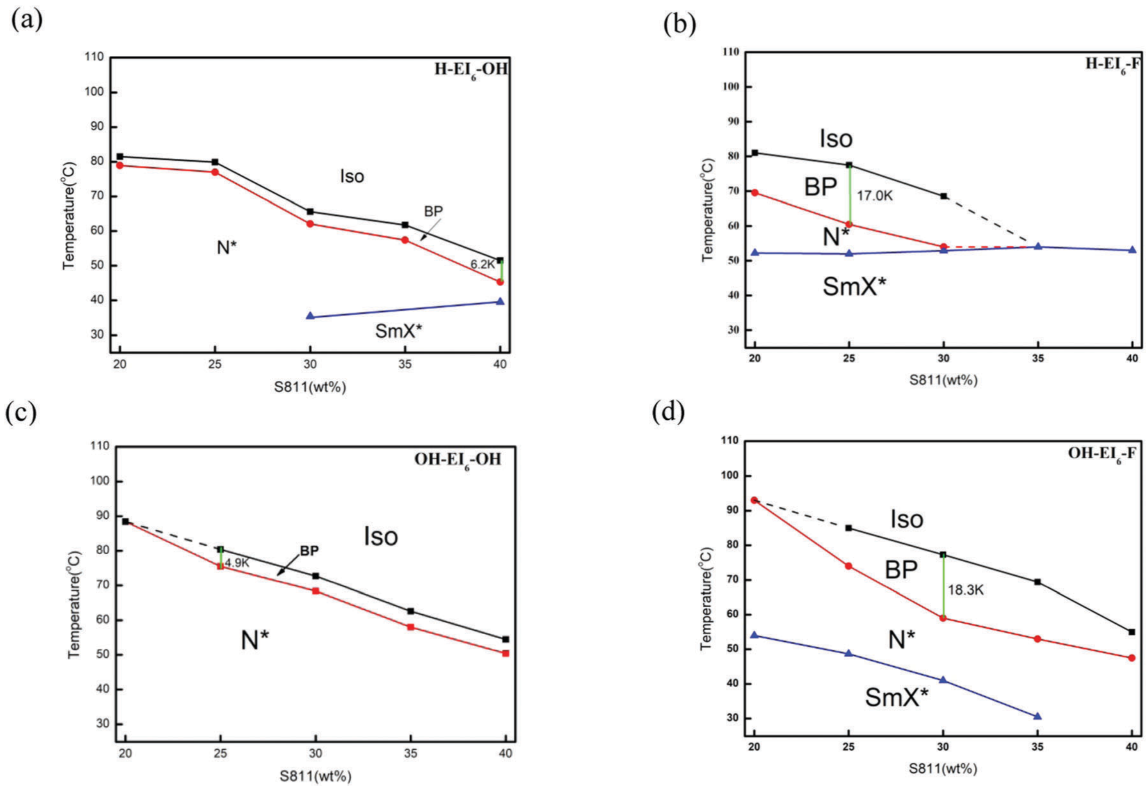

Fig. 4 Phase diagrams of (a) **H-EI$_6$-OH**; (b) **H-EI$_6$-F**; (c) **OH-EI$_6$-OH**; (d) **OH-EI$_6$-F** when doped with different concentrations of chiral dopant **S811** at a cooling rate of 0.2 °C min^{-1}. Iso, BP, N*, SmX* and Cr indicate isotropic phase, blue phase, cholesteric phase, smectic phase and crystal phase, respectively.

Table 2 Phase transitions in binary mixture of Schiff base mesogens of type **I** doped with different concentrations of chiral dopant **ISO(6OBA)$_2$** at a cooling rate of 0.2 °C min^{-1} [a]

Compound	wt%	Phase behavior	$\Delta BP_{cooling}$ (K)	Compound	wt%	Phase behavior	$\Delta BP_{cooling}$ (K)
H-EI$_6$-OH	5	$\mathrm{Cr} \underset{<27.0}{\overset{<27.0}{\rightleftharpoons}} \mathrm{N}^* \underset{98.6}{\overset{98.4}{\rightleftharpoons}} \mathrm{Iso}$	0.0	**OH-EI$_6$-OH**	5	$\mathrm{Cr} \underset{<27.0}{\overset{<27.0}{\rightleftharpoons}} \mathrm{N}^* \underset{107.3}{\overset{107.8}{\rightleftharpoons}} \mathrm{Iso}$	0.0
	10	$\mathrm{Cr} \underset{<27.0}{\overset{<27.0}{\rightleftharpoons}} \mathrm{N}^* \underset{85.6}{\overset{87.6}{\rightleftharpoons}} \mathrm{BP} \underset{91.1}{\overset{91.3}{\rightleftharpoons}} \mathrm{Iso}$	5.5		10	$\mathrm{Cr} \underset{<27.0}{\overset{<27.0}{\rightleftharpoons}} \mathrm{N}^* \underset{85.8}{\overset{88.5}{\rightleftharpoons}} \mathrm{BP} \underset{95.0}{\overset{95.2}{\rightleftharpoons}} \mathrm{Iso}$	9.2
	15	$\mathrm{Cr} \underset{<27.0}{\overset{<27.0}{\rightleftharpoons}} \mathrm{N}^* \underset{76.5}{\overset{77.4}{\rightleftharpoons}} \mathrm{BP} \underset{83.2}{\overset{79.4}{\rightleftharpoons}} \mathrm{Iso}$	6.7		15	$\mathrm{Cr} \underset{<27.0}{\overset{<27.0}{\rightleftharpoons}} \mathrm{N}^* \underset{81.6}{\overset{70.2}{\rightleftharpoons}} \mathrm{Iso}$	0.0
H-EI$_6$-F	5	$\mathrm{Cr} \underset{<27.0}{\overset{<27.0}{\rightleftharpoons}} \mathrm{N}^* \underset{96.1}{\overset{96.5}{\rightleftharpoons}} \mathrm{Iso}$	0.0	**OH-EI$_6$-F**	5	$\mathrm{Cr} \underset{<40.0}{\overset{<40.0}{\rightleftharpoons}} \mathrm{N}^* \underset{115.4}{\overset{115.8}{\rightleftharpoons}} \mathrm{Iso}$	0.0
	10	$\mathrm{Cr} \underset{<27.0}{\overset{<27.0}{\rightleftharpoons}} \mathrm{N}^* \underset{55.4}{\overset{63.7}{\rightleftharpoons}} \mathrm{BP} \underset{77.2}{\overset{83.1}{\rightleftharpoons}} \mathrm{Iso}$	21.8		10	$\mathrm{Cr} \underset{34.6}{\overset{34.6}{\rightleftharpoons}} \mathrm{N}^* \underset{111.4}{\overset{111.6}{\rightleftharpoons}} \mathrm{Iso}$	0.0
	15	$\mathrm{Cr} \underset{<27.0}{\overset{<27.0}{\rightleftharpoons}} \mathrm{N}^* \underset{54.4}{\overset{62.8}{\rightleftharpoons}} \mathrm{BP} \underset{75.5}{\overset{84.3}{\rightleftharpoons}} \mathrm{Iso}$	21.1		15	$\mathrm{Cr} \underset{32.0}{\overset{32.0}{\rightleftharpoons}} \mathrm{N}^* \underset{105.0}{\overset{105.6}{\rightleftharpoons}} \mathrm{Iso}$	0.0

[a] Iso = isotropic; BP = blue phase; N* = chiral nematic; Cr = crystal phase.

temperatures increased. In addition, Table 2 displays the phase transition temperature and BP range for Schiff base mesogens **I** doped with 5–15 wt% chiral dopant **ISO(6OBA)$_2$**. In the case of a binary mixture consisting of 90 wt% Schiff base mesogen **H-EI$_6$-F** and 10 wt% **ISO(6OBA)$_2$**, the BP range can be increased to more than 20 K as well as its BP emerging temperature being lower than that of the binary mixture consisting of no fluoro-substituted **H-EI$_6$**. However, no BP can be observed in the binary mixture composed of difluoro-substituted Schiff base mesogen **OH-EI$_6$-F**. This phenomenon is similar to the binary mixture containing Schiff base mesogen **OH-EI$_6$** under the same chirality condition. However, a BP emerges again (9.2 K) in the case of Schiff base mesogen **OH-EI$_6$-OH** possessing two intramolecular hydrogen bonds by two hydroxy groups with the ester and imine linkages.

Fig. 5 shows the phase diagrams of rodlike Schiff base mesogens **III** mixed with 20–40 wt% concentrations of chiral

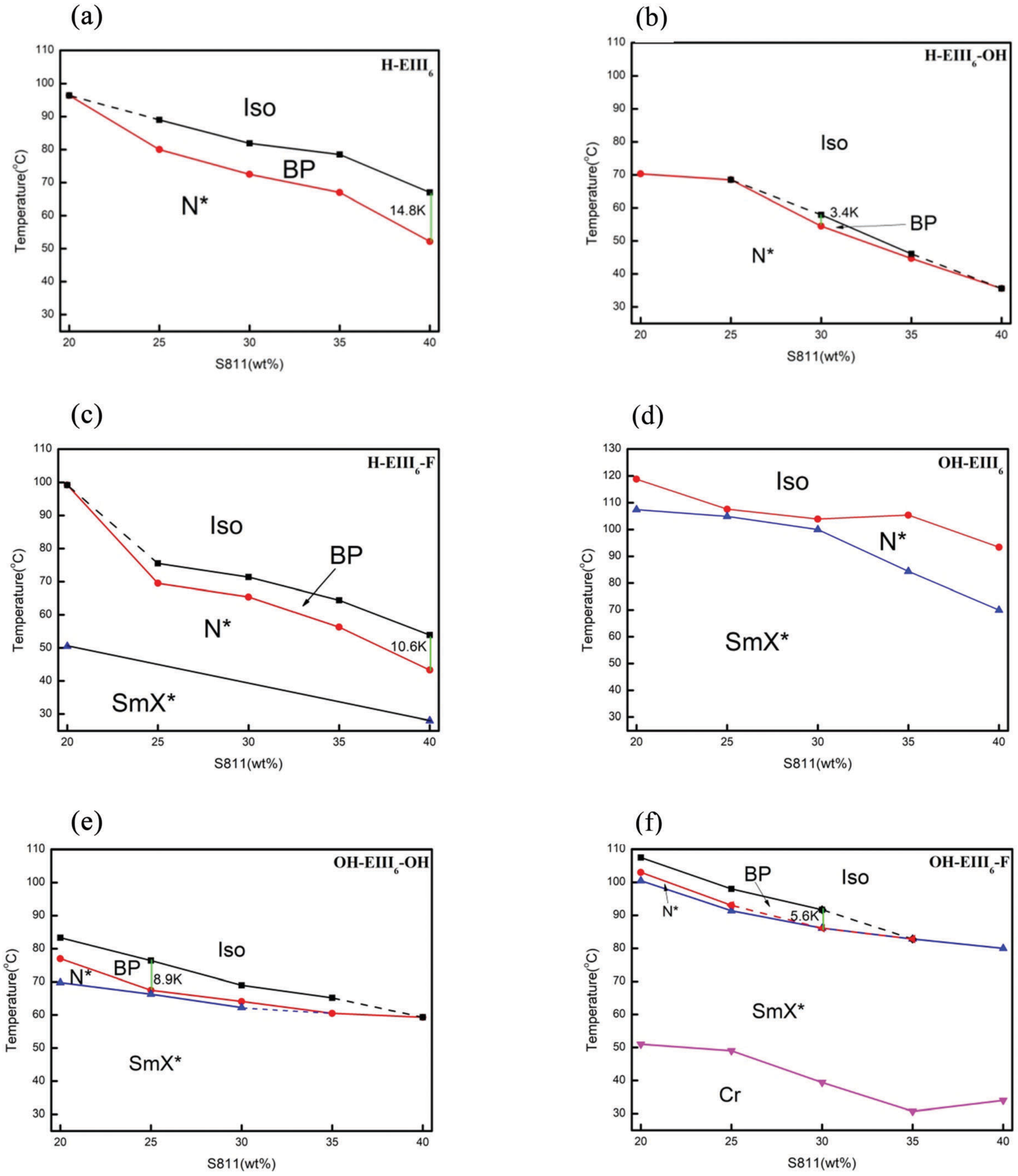

Fig. 5 Phase diagrams of (a) **H-EIII$_6$**; (b) **H-EIII$_6$-OH**; (c) **H-EIII$_6$-F**; (d) **OH-EIII$_6$**; (e) **OH-EIII$_6$-OH**; (f) **OH-EIII$_6$-F** when doped with different concentrations of chiral dopant **S811** at a cooling rate of 0.2 °C min^{-1}. Iso, BP, N*, SmX* and Cr indicate isotropic phase, blue phase, cholesteric phase, smectic phase and crystal phase, respectively.

Table 3 Phase transitions in a binary mixture of Schiff base mesogens of type **III** doped with different concentrations of chiral dopant **ISO(6OBA)$_2$** at a cooling rate of 0.2 °C min^{-1a}

Compound	wt%	Phase behavior	$\Delta BP_{cooling}$ (K)	Compound	wt%	Phase behavior	$\Delta BP_{cooling}$ (K)
H-EIII$_6$	5	$\mathrm{Cr}\ \underset{<27.0}{\overset{<27.0}{\rightleftharpoons}}\ \mathrm{N}^*\ \underset{114.4}{\overset{116.5}{\rightleftharpoons}}\ \mathrm{Iso}$	0.0	**OH-EIII$_6$**	5	$\mathrm{Cr}\ \underset{<27.0}{\overset{<27.0}{\rightleftharpoons}}\ \mathrm{SmX}^*\ \underset{114.5}{\overset{112.2}{\rightleftharpoons}}\ \mathrm{N}^*\ \underset{145.1}{\overset{143.8}{\rightleftharpoons}}\ \mathrm{Iso}$	0.0
	10	$\mathrm{Cr}\ \underset{<27.0}{\overset{<27.0}{\rightleftharpoons}}\ \mathrm{N}^*\ \underset{103.3}{\overset{104.9}{\rightleftharpoons}}\ \mathrm{Iso}$	0.0		10	$\mathrm{Cr}\ \underset{<27.0}{\overset{<27.0}{\rightleftharpoons}}\ \mathrm{SmX}^*\ \underset{102.5}{\overset{103.7}{\rightleftharpoons}}\ \mathrm{N}^*\ \underset{140.1}{\overset{141.5}{\rightleftharpoons}}\ \mathrm{Iso}$	0.0
	15	$\mathrm{Cr}\ \underset{38.1}{\overset{38.1}{\rightleftharpoons}}\ \mathrm{N}^*\ \underset{93.2}{\overset{95.0}{\rightleftharpoons}}\ \mathrm{Iso}$	0.0		15	$\mathrm{Cr}\ \underset{<27.0}{\overset{<27.0}{\rightleftharpoons}}\ \mathrm{SmX}^*\ \underset{97.7}{\overset{98.6}{\rightleftharpoons}}\ \mathrm{N}^*\ \underset{135.1}{\overset{135.5}{\rightleftharpoons}}\ \mathrm{Iso}$	0.0
H-EIII$_6$-OH	5	$\mathrm{Cr}\ \underset{<27.0}{\overset{<27.0}{\rightleftharpoons}}\ \mathrm{N}^*\ \underset{82.1}{\overset{81.0}{\rightleftharpoons}}\ \mathrm{Iso}$	0.0	**OH-EIII$_6$-OH**	5	$\mathrm{Cr}\ \underset{<27.0}{\overset{<27.0}{\rightleftharpoons}}\ \mathrm{N}^*\ \underset{93.9}{\overset{95.6}{\rightleftharpoons}}\ \mathrm{BP}\ \underset{99.3}{\overset{99.5}{\rightleftharpoons}}\ \mathrm{Iso}$	5.4
	10	$\mathrm{Cr}\ \underset{<27.0}{\overset{<27.0}{\rightleftharpoons}}\ \mathrm{N}^*\ \underset{75.7}{\overset{75.7}{\rightleftharpoons}}\ \mathrm{Iso}$	0.0		10	$\mathrm{Cr}\ \underset{<27.0}{\overset{<27.0}{\rightleftharpoons}}\ \mathrm{N}^*\ \underset{80.6}{\overset{81.0}{\rightleftharpoons}}\ \mathrm{Iso}$	0
	15	$\mathrm{Cr}\ \underset{<27.0}{\overset{<27.0}{\rightleftharpoons}}\ \mathrm{N}^*\ \underset{50.9}{\overset{53.9}{\rightleftharpoons}}\ \mathrm{Iso}$	0.0		15	$\mathrm{Cr}\ \underset{<27.0}{\overset{<27.0}{\rightleftharpoons}}\ \mathrm{N}^*\ \underset{55.0}{\overset{59.5}{\rightleftharpoons}}\ \mathrm{Iso}$	0.0
H-EIII$_6$-F	5	$\mathrm{Cr}\ \underset{<27.0}{\overset{<27.0}{\rightleftharpoons}}\ \mathrm{N}^*\ \underset{105.7}{\overset{105.0}{\rightleftharpoons}}\ \mathrm{Iso}$	0.0	**OH-EIII$_6$-F**	5	$\mathrm{Cr}\ \underset{62.5}{\overset{62.5}{\rightleftharpoons}}\ \mathrm{SmX}^*\ \underset{91.1}{\overset{91.7}{\rightleftharpoons}}\ \mathrm{N}^*\ \underset{128.5}{\overset{126.0}{\rightleftharpoons}}\ \mathrm{Iso}$	0.0
	10	$\mathrm{Cr}\ \underset{<27.0}{\overset{<27.0}{\rightleftharpoons}}\ \mathrm{N}^*\ \underset{75.3}{\overset{78.5}{\rightleftharpoons}}\ \mathrm{BP}\ \underset{89.5}{\overset{89.4}{\rightleftharpoons}}\ \mathrm{Iso}$	14.2		10	$\mathrm{Cr}\ \underset{62.2}{\overset{62.5}{\rightleftharpoons}}\ \mathrm{SmX}^*\ \underset{92.5}{\overset{93.1}{\rightleftharpoons}}\ \mathrm{N}^*\ \underset{110.5}{\overset{118.0}{\rightleftharpoons}}\ \mathrm{BP}\ \underset{124.7}{\overset{122.5}{\rightleftharpoons}}\ \mathrm{Iso}$	14.2
	15	$\mathrm{Cr}\ \underset{<27.0}{\overset{<27.0}{\rightleftharpoons}}\ \mathrm{N}^*\ \underset{63.2}{\overset{81.5}{\rightleftharpoons}}\ \mathrm{BP}\ \underset{85.0}{\overset{91.0}{\rightleftharpoons}}\ \mathrm{Iso}$	21.8		15	$\mathrm{Cr}\ \underset{61.3}{\overset{61.3}{\rightleftharpoons}}\ \mathrm{SmX}^*\ \underset{88.2}{\overset{89.0}{\rightleftharpoons}}\ \mathrm{N}^*\ \underset{92.0}{\overset{101.3}{\rightleftharpoons}}\ \mathrm{BP}\ \underset{107.5}{\overset{110.0}{\rightleftharpoons}}\ \mathrm{Iso}$	15.5

[a] Iso = isotropic; BP = blue phase; N* = chiral nematic; SmX* = unidentified chiral smectic phase; Cr = crystal phase.

dopant **S811** and Table 3 displays their phase transition temperatures and BP ranges with 5–15 wt% concentrations of chiral dopant **ISO(6OBA)$_2$**. The results show that the BP emerging temperatures in these binary mixtures are higher than those containing Schiff base mesogens **I**. Schiff base mesogen **H-EIII$_6$** possessing no hydroxy group exhibits a BP range of approximately 15 K in the binary mixture where chiral dopant **S811** is increased to 40 wt%. Notably, Schiff base mesogen **OH-EIII$_6$** cannot induce a BP under any chirality condition even though its molecular structure is similar to Schiff base mesogen **OH-EI$_6$**, possessing intramolecular hydrogen bonding between the hydroxy group and the imine linkage. In the case of the binary mixture with chiral dopant **ISO(6OBA)$_2$**, a BP can be observed only in the binary mixture composed of Schiff base mesogens **H-EIII$_6$-F**, **OH-EIII$_6$-OH** or **OH-EIII$_6$-F** having two hydroxy or fluoro substituents. The widest BP range that can be induced is more than 20 K when 15 wt% **ISO(6OBA)$_2$** is added into Schiff base mesogen **H-EIII$_6$-F**. And the doping concentration of chiral dopant **ISO(6OBA)$_2$** that can induce a wider BP range (> 20 K) for Schiff base mesogen **H-EIII$_6$-F** is higher than that for Schiff base mesogen **H-EI$_6$-F** (10 wt% **ISO(6OBA)$_2$**).

The study on the phase transition between BPI and BPII with reflection measurements. To precisely identify the boundaries of cubic BPs, the temperature dependence of the Bragg reflection spectrum for these BP binary mixtures was examined. Fig. 6–9 and Fig. S9–S27 (ESI†) display the typical temperature dependence of the Bragg reflection wavelength for two types of Schiff base mesogens being doped with appropriate concentrations of chiral dopants **S811** or **ISO(6OBA)$_2$** during cooling (0.2 °C min^{-1}). According to our previous report,[42,43] BPI and BPII can be observed when the binary mixture is composed of 35 wt% **S811** and 65 wt% Schiff base mesogen **OH-EI$_6$** possessing a hydroxy group near the imine linkage. However, Fig. 6a shows only a single reflection band around 420 nm during cooling, indicating only BPII is present when chiral dopant **S811** is doped into Schiff base mesogen **H-EI$_6$-OH** possessing a hydroxy group near the ester linkage. In addition, a similar selective reflection peak of BPII can also be observed during cooling and heating processes when difluoro substituted Schiff base mesogen **H-EI$_6$-F** is doped with 30 wt% **S811** (Fig. S9 and S10, ESI†). In the case of Schiff base mesogen **OH-EI$_6$-F** being doped with 30 wt% **S811**, only a single reflection band around 450 nm shown in Fig. 7 can be observed at 75 °C, indicating that BPII with the (100) direction exists in the higher BP temperature range. On further cooling to 70 °C, another broad reflection band appeared at approximately 510 nm and it exhibits an obvious red shift from 510 nm to 655 nm during cooling, indicating the characteristics of the BPI phase caused by the multi-lattice plane orientations of the different platelet domains. The two reflection bands are associated with the (200) and (110) directions of the cubic lattice vectors for nanostructured BPI.[13] Therefore, the pictures of POM shown in the insets of Fig. 7b gradually change from a blue platelet texture to a grazed colorful platelet texture during the cooling process. Notably, in the case of Schiff base mesogen **OH-EI$_6$-OH** being doped with 25 wt% **S811**, two selective reflection peaks appear as BPI characteristics in the higher temperature range (Fig. S11, ESI†). On further cooling to 77 °C, broader multiple reflection peaks can be observed possibly due to the multi-lattice plane orientations of the different platelet domains in the lower temperature range.[54–56] As for Schiff base mesogens **I** being doped with chiral additive **ISO(6OBA)$_2$**, only BPII is present in the binary mixture consisting of Schiff base mesogens **H-EI$_6$-OH**, **OH-EI$_6$-OH** and **H-EI$_6$-F** both on cooling and heating (Fig. S12–S16, ESI†).

As for Schiff base mesogens **III**, Schiff base mesogens **H-EIII$_6$-OH** and **OH-EIII$_6$-OH** possessing a hydroxy group near the ester linkage exhibit BPII on cooling after an appropriate concentration of **S811** is added into them (Fig. S18 and S19, ESI†). Similar characteristics of BPII can be observed in the case of difluoro substituted Schiff base mesogen **OH-EIII$_6$-F** both on cooling and heating (Fig. S20 and S21, ESI†). However, in the

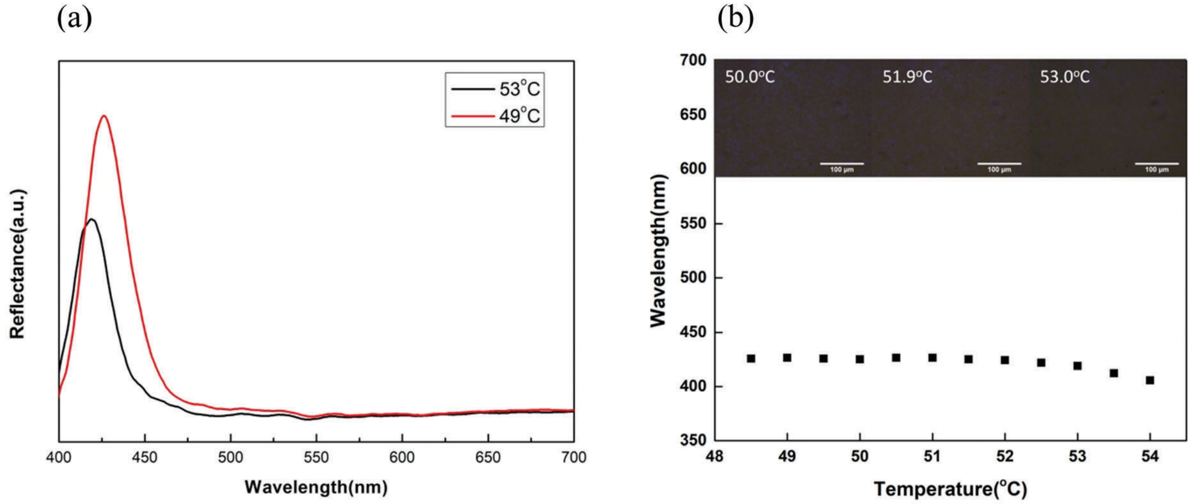

Fig. 6 (a) Typical shapes of the reflection spectra. (b) The temperature dependence of the Bragg reflection wavelength for the blending mixture consisting of **H-EI$_6$-OH** + 40% **S811** at a cooling rate of 0.2 °C min^{-1}. Insets show the POM images of BPs at different temperatures.

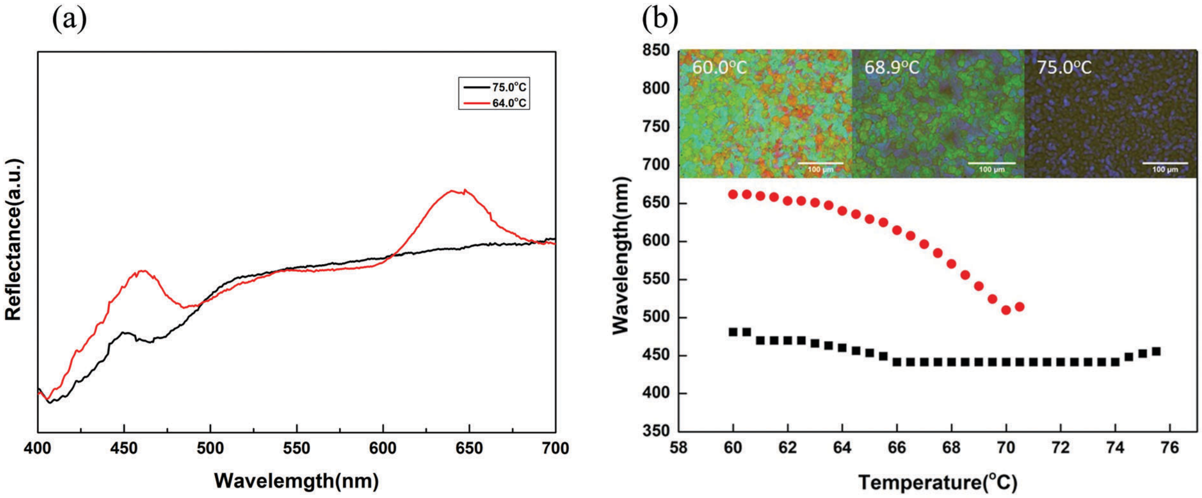

Fig. 7 (a) Typical shapes of the reflection spectra. (b) The temperature dependence of the Bragg reflection wavelength for the blending mixture consisting of **OH-EI$_6$-F** + 30% **S811** at a cooling rate of 0.2 °C min^{-1}. Insets show the POM images of BPs at different temperatures.

case of difluoro substituted Schiff base mesogen **H-EIII$_6$-F** being doped with 35% **S811**, Fig. 8b obviously shows a discontinuous jump at around 63 °C and a selective reflection peak exhibits an apparent red shift from 460 nm to 510 nm in the temperature dependence on cooling, indicating a typical transition between BPI and BPII. In contrast to **OH-EI$_6$-F**, the BPI of Schiff base mesogen **H-EIII$_6$-F** shows that only one reflection band at approximately 510 nm is associated with the (200) direction.[13] However, one reflection band with another direction (110) of BPI cannot be observed possibly due to the weaker intensity of the grazed iridescent platelet for the BP domain of Schiff base mesogen **H-EIII$_6$-F.**[54] When Schiff base mesogens **III** are doped with chiral dopant **ISO(6OBA)$_2$**, BPII can be observed only in the cases of **H-EIII$_6$-F**, **OH-EIII$_6$-OH** and **OH-EIII$_6$-F** on cooling. Interestingly, Fig. 9 and Fig. S26 (ESI†) exhibit two reflection bands as BPI characteristics can be observed on heating in the cases of the difluoro substituted Schiff base mesogens **OH-EIII$_6$-F** and **H-EIII$_6$-F**.

Theoretical simulation. According to our previous investigations for the factors of BP stabilization, the range-corrected functional CAM-B3LYP[51] was applied to analyze the structural variations of Schiff base mesogens and obtain the stable molecular structure, dipole moment, polarizability and biaxiality. The optimized molecular structures together with the vector of dipole moments are shown in Fig. 10. The correlations of BP stabilization with the differences of biaxiality, modulus of dipole moments and polarizability in the optimized Schiff base mesogens are shown in Tables 4 and 5. The biaxiality (W_1/W_2) is defined as the ratio of two distinguishable short axes of the molecule. W_1 is the width along the short axis parallel to the middle phenyl ring and W_2 is the width along the short axis normal to the middle phenyl ring. In addition, the detailed

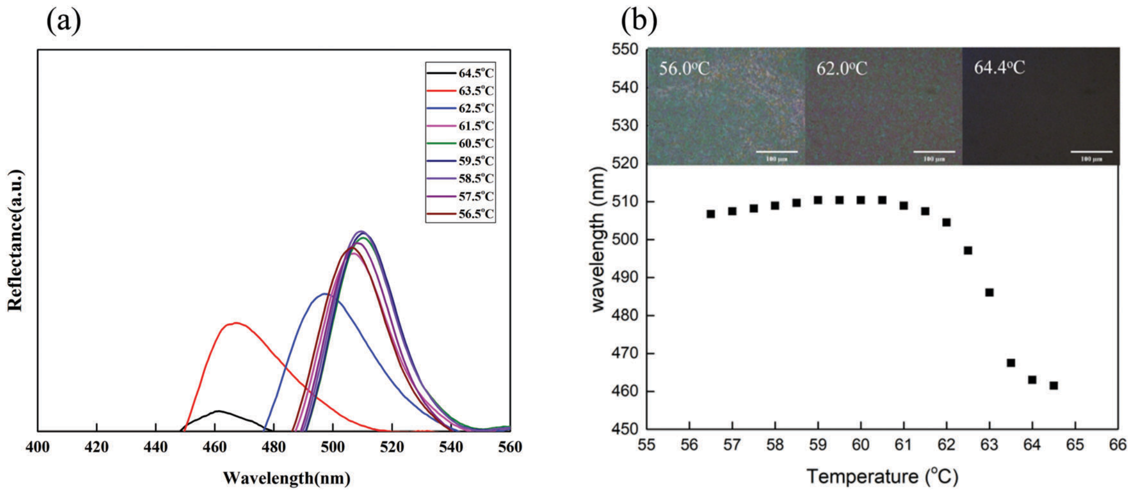

Fig. 8 (a) Typical shapes of the reflection spectra. (b) The temperature dependence of the Bragg reflection wavelength for the blending mixture consisting of **H-EIII$_6$-F** + 35% **S811** at a cooling rate of 0.2 °C min^{-1}. Insets show the POM images of BPs at different temperatures.

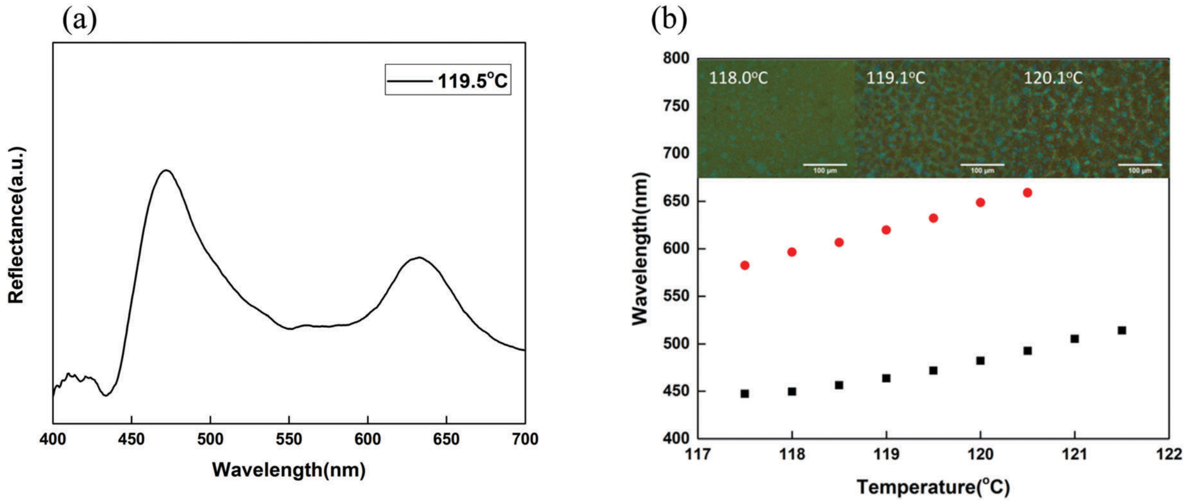

Fig. 9 (a) A typical shape of the reflection spectrum. (b) The temperature dependence of the Bragg reflection wavelength for the blending mixture consisting of **OH-EIII$_6$-F** + 10% **ISO(6OBA)$_2$** at a heating rate of 0.2 °C min^{-1}. Insets show the POM images of BPs at different temperatures.

information of each component of dipole moment, polarizability, and the energy of the HOMO and LUMO are listed in Table S1 (ESI†). To facilitate the comparisons with those factors of BP stabilization based on structural similarity, the molecular structures of Schiff base mesogens **H-EI$_6$** and **OH-EI$_6$** that have been prepared previously were also calculated and their factors are also listed in Tables 4 and 5, respectively.

Table 4 shows the correlations of BP range with the differences of biaxiality, modulus of dipole moments and polarizability for optimized Schiff base mesogens possessing no hydroxy group near the imine linkage. In comparison with Schiff base mesogen **H-EI$_6$**, two fluoro substituted Schiff base mesogen **H-EI$_6$-F** possesses a larger dipole moment and polarizability due to the incorporation of two fluorine atoms. Therefore, **H-EI$_6$-F** in the binary mixture system containing 30 wt% **S811** or 10 wt% **ISO(6OBA)$_2$** shows a wider BP range than that of **H-EI$_6$** under the same chirality condition. Similar trends can be observed in the binary mixtures composed of two fluoro substituted Schiff base mesogens **III** possessing no hydroxy group near the imine linkage. With a hydroxy group near the ester linkage, the dipole moment of Schiff base mesogen **H-EI$_6$-OH** (2.80 D) is smaller than those of Schiff base mesogens **H-EI$_6$** (2.95 D) and **H-EI$_6$-F** (4.58 D). Subsequently, Schiff base mesogen **H-EI$_6$-OH** exhibits a narrower BP range than **H-EI$_6$** and **H-EI$_6$-F**. Notably, when Schiff base mesogen **H-EIII$_6$** is doped with 30 wt% **S811**, it exhibits a BP range (9.4 K) due to its large biaxiality (1.45) even though it possesses a small dipole moment (0.64 D). However, the dipole moment and polarizability of **H-EIII$_6$** are smaller than those of **H-EIII$_6$-F**, so that a BP cannot be induced in the binary mixture with 10 wt% **ISO(6OBA)$_2$**. In addition, the dipole moment and polarizability of Schiff base mesogen **H-EIII$_6$-OH** are larger than those of its homologues **H-EIII$_6$** and **H-EIII$_6$-F**. Nevertheless, when **H-EIII$_6$-OH** is doped with

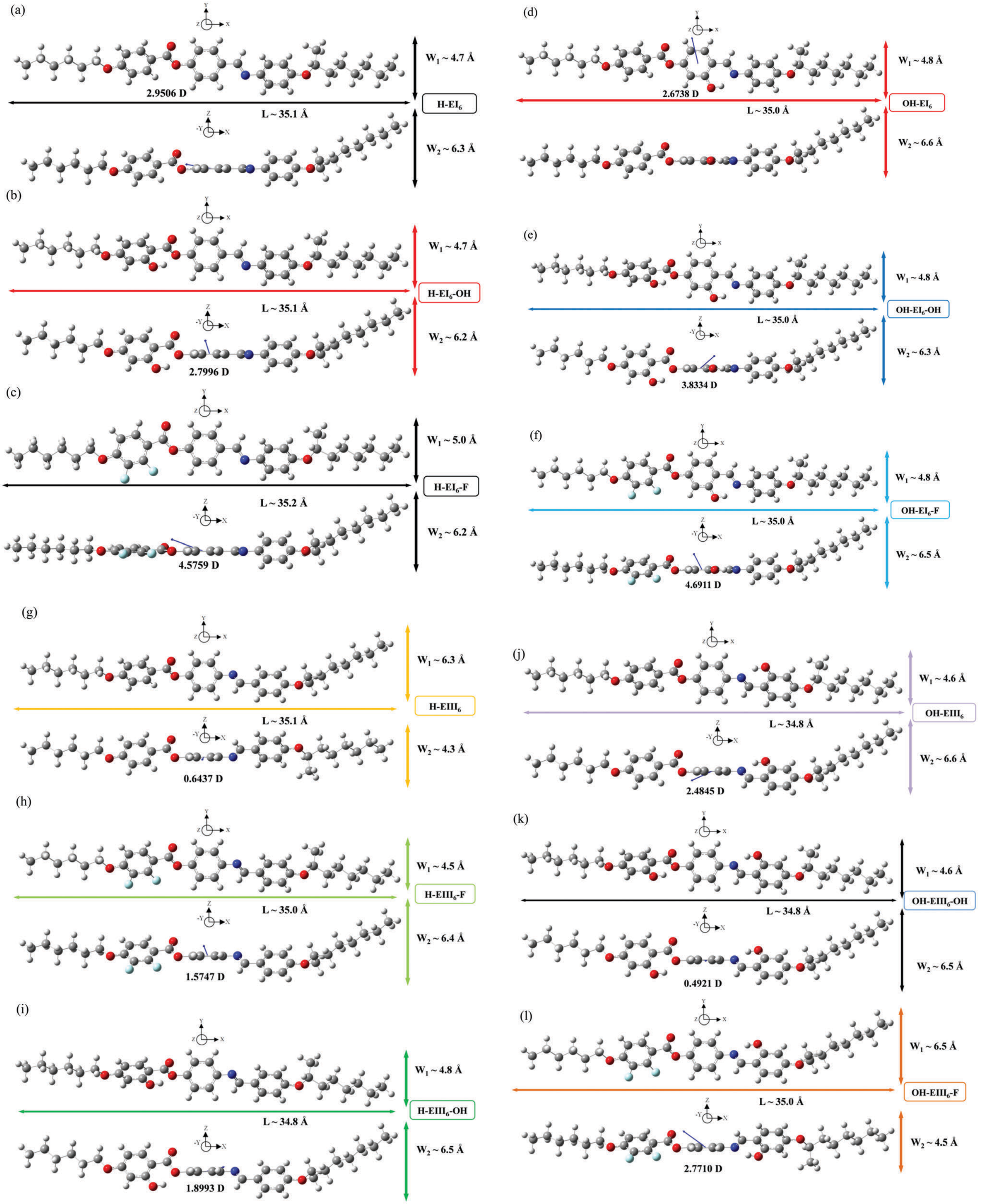

Fig. 10 The optimized molecular structures of Schiff base mesogens (a) **H-EI$_6$**; (b) **H-EI$_6$-F**; (c) **H-EI$_6$-OH**; (d) **OH-EI$_6$**; (e) **OH-EI$_6$-F**; (f) **OH-EI$_6$-OH**; (g) **H-EIII$_6$**; (h) **H-EIII$_6$-F**; (i) **H-EIII$_6$-OH**; (j) **OH-EIII$_6$**; (k) **OH-EIII$_6$-F**; (l) **OH-EIII$_6$-OH** together with their each corresponding molecular dimensions and dipole moment indicated by the blue arrow.

Table 4 The correlations of BP range with the differences of biaxiality, modulus of dipole moments and polarizability for optimized Schiff base mesogens possessing no hydroxy group near the imine linkage

Compound	**H-EI$_6$**	**H-EI$_6$-F**	**H-EI$_6$-OH**	**H-EIII$_6$**	**H-EIII$_6$-F**	**H-EIII$_6$-OH**
Dipole moment (Debye)	2.95	4.58	2.80	0.64	1.57	1.90
Polarizability	445.84	448.08	450.73	444.02	445.19	449.49
W_1[a] (Å)	4.7	5.0	4.7	4.3	4.5	4.8
W_2[b] (Å)	6.3	6.2	6.2	6.3	6.4	6.5
Biaxiality W_1/W_2	0.75	0.81	0.77	1.45	0.70	0.74
L[c] (Å)	35.1	35.2	35.1	35.1	35.0	34.8
The BP range (K) with 30 wt% **S811**	12.1	17.0	3.5	9.4	10.6	3.4
The BP range (K) with 10 wt% **ISO(6OBA)$_2$**	7.1	21.8	5.5	0.0	14.2	0.0

[a] W_1: width along the short axis parallel to the middle phenyl ring. [b] W_2: width along the short axis normal to the middle phenyl ring. [c] L: length along the long axis.

Table 5 The correlations of BP range with the differences of biaxiality, modulus of dipole moments and polarizability for optimized Schiff base mesogens possessing a hydroxy group near the imine linkage

Compound	**OH-EI$_6$**	**OH-EI$_6$-F**	**OH-EI$_6$-OH**	**OH-EIII$_6$**	**OH-EIII$_6$-F**	**OH-EIII$_6$-OH**
Dipole moment (Debye)	2.67	4.69	3.83	2.48	2.71	0.49
Polarizability	465.55	453.81	457.82	453.06	454.44	458.46
W_1[a] (Å)	4.8	4.8	4.8	4.6	4.5	4.6
W_2[b] (Å)	6.6	6.5	6.3	6.6	6.5	6.5
Biaxiality W_1/W_2	0.73	0.74	0.76	0.70	1.45	0.70
L[c] (Å)	35.0	35.0	35.0	34.8	35.0	34.8
The BP range (K) with 30 wt% **S811**	7.4	18.3	4.3	0.0	5.6	4.9
The BP range (K) with 10 wt% **ISO(6OBA)$_2$**	0.0	0.0	9.2	0.0	14.2	0.0

[a] W_1: width along the short axis parallel to the middle phenyl ring. [b] W_2: width along the short axis normal to the middle phenyl ring. [c] L: length along the long axis.

30 wt% **S811,** it exhibits a narrow BP range (3.4 K). And no BP can be induced when **H-EIII$_6$-OH** is doped with 10 wt% **ISO(6OBA)$_2$**.

In the case of Schiff base mesogen **I** possessing a hydroxy group the near imine linkage, Schiff base mesogens **OH-EI$_6$-F** and **OH-EI$_6$-OH** show larger dipole moments in comparison with Schiff base mesogen **OH-EI$_6$** by reason of the incorporation of two fluorine atoms and a hydroxy group near the ester linkage, respectively. Thus, Schiff base mesogen **OH-EI$_6$-F** in the binary mixture system with 30 wt% **S811** shows a wider BP range (18.3 K) than that of **OH-EI$_6$** (7.4 K) under the same chirality condition. However, Schiff base mesogen **OH-EI$_6$-F** cannot induce a BP when it is doped with **ISO(6OBA)$_2$**. This phenomenon is similar to that of **OH-EI$_6$** under the same chirality condition. Unexpectedly, a BP (9.2 K) emerges when Schiff base mesogen **OH-EI$_6$-OH** is doped with 10 wt% **ISO(6OBA)$_2$** possibly due to its larger biaxiality. As for Schiff base mesogens **III**, two fluoro substituted Schiff base mesogen **OH-EIII$_6$-F** possesses larger biaxiality, dipole moments and slightly lager polarizability than Schiff base mesogens **OH-EIII$_6$** and **OH-EIII$_6$-OH**. Thus, a BP emerges easily when two fluoro substituted Schiff base mesogen **OH-EIII$_6$-F** is doped with 30 wt% **S811** or 10 wt% **ISO(6OBA)$_2$**. However, in comparison with Schiff base mesogens **I**, the dipole moment of Schiff base mesogen **OH-EIII$_6$-OH** (0.49 D) possessing two hydroxy groups is smaller than that of **OH-EI$_6$-OH** (3.83 D), so that the BP disappears when **OH-EIII$_6$-OH** is doped with chiral dopant **ISO(6OBA)$_2$**. Accordingly, except for **OH-EI$_6$** doped with **ISO(6OBA)$_2$**, the main factor in BP stabilization is the dipole moment for Schiff base mesogens **I** in the chiral system. However, for Schiff base mesogens **III**, the fluorine substituent effect is dominant for BP stabilization.

4. Conclusion

In conclusion, two series of racemic rodlike Schiff base mesogens that possess –C=N– (type **I**) and –N=C– (type **III**) linkages were synthesized, respectively. Their mesophases were confirmed by variable-temperature XRD, DSC and the characteristic texture of POM. Subsequently, the effects of intramolecular hydrogen bonding *via* the hydroxy group with ester or Schiff base linkages, and difluoro substitutions at the inner-core position of the phenyl ring on BP stabilization were investigated when they were blended with chiral dopants **S811** or **ISO(6OBA)$_2$**. The incorporation of difluoro substitutions into the inner-core position of the phenyl ring or intramolecular hydrogen bonding *via* the hydroxy group with the ester in Schiff base mesogens results in the BP formation temperature decreasing in the binary mixture. The presence of two fluoro substituents protruding from the side of the mesogenic core is more beneficial for BP stabilization than that of intramolecular hydrogen bonding between a hydroxy group and the ester linkage in the Schiff base mesogen. The phase transition between BPI and BPII can be confirmed by measuring the temperature dependence of the Bragg reflection and POM. Schiff base mesogens possessing only a hydroxy group near the ester linkage easily exhibit BPII in the binary mixture containing chiral dopant **S811** on cooling. In addition, only BPII can be induced when chiral dopant **ISO(6OBA)$_2$** is doped into the Schiff base mesogen during the cooling process. Interestingly, BPI can be observed in the binary mixture of two difluoro substituted Schiff base mesogens **III** being doped with 10–15 wt% chiral dopant **ISO(6OBA)$_2$** on heating. Based on the molecular modeling, we demonstrated that a wider BP range can be induced when two difluoro substituted Schiff base mesogens that possess larger dipole moments are doped with appropriate concentrations of chiral dopants **S811** or **ISO(6OBA)$_2$**. In addition, the dipole moments of Schiff base mesogens **I** are larger than those of Schiff base mesogens **III**. Consequently, it is concluded that BPs can be induced for racemic rodlike Schiff base mesogens **I** in a chiral system and it is easier than that for racemic rodlike Schiff base mesogens **III**. In addition, the presence of two fluoro substituents in the racemic rodlike Schiff base mesogens is the main factor that affects BP stabilization for Schiff base mesogens **III** in a chiral system. This work reports the effects of molecular structure and functional group of racemic rodlike Schiff base mesogens on BP stabilization under chiral conditions. Moreover, it also offers possible approaches for the use of the difluoro substituted Schiff base mesogen **H-EI$_6$-F** as a host to be diluted with nematic LCs, which may be used for future applications of room-temperature eutectic liquid crystal mixtures with wide BP ranges.

Conflicts of interest

There are no conflicts to declare.

Acknowledgements

This research was supported by the Ministry of Science and Technology through MOST 106-2113-M-036-001, MOST 106-2113-M-027-002, and Tatung University through B107-C04-010, Taiwan. In addition, we particularly thank Mr Chang-Yu Chou and Ms Pei-Yi Shih for assisting in the synthesis of some precursors of these Schiff base mesogens.

References

1 L. Rao, Z. Ge and S. T. Wu, *Opt. Express*, 2010, **18**, 3143–3148.
2 J. Yan, S.-T. Wu, K.-L. Cheng and J.-W. Shiu, *Appl. Phys. Lett.*, 2013, **102**, 081102.
3 J. Yan and S.-T. Wu, *Opt. Mater. Express*, 2011, **1**, 1527–1535.
4 Y. Chen and S.-T. Wu, *J. Appl. Polym. Sci.*, 2014, **131**, 40556.
5 L. Rao, Z. Ge, S.-T. Wu and S. H. Lee, *Appl. Phys. Lett.*, 2009, **95**, 231101.
6 J. Yan, L. Rao, M. Jiao, Y. Li, H.-C. Cheng and S.-T. Wu, *J. Mater. Chem.*, 2011, **21**, 7870–7877.
7 M. Lee, S. T. Hur, H. Higuchi, K. Song, S.-W. Choi and H. Kikuchi, *J. Mater. Chem.*, 2010, **20**, 5813–5816.
8 Z. Ge, L. Rao, S. Gauza and S.-T. Wu, *J. Disp. Technol.*, 2009, **5**, 250–256.
9 L. Rao, Z. Ge, S. Gauza, K.-M. Chen and S.-T. Wu, *Mol. Cryst. Liq. Cryst.*, 2010, **527**, 30–42.
10 L. Rao and S.-T. Wu, *Liq. Cryst. Today*, 2014, **24**, 3–12.
11 Z. B. Ge, S. Gauza, M. Z. Jiao, H. Q. Xianyu and S. T. Wu, *Appl. Phys. Lett.*, 2009, **94**, 101104.
12 M. Jiao, Y. Li and S.-T. Wu, *Opt. Lett.*, 2011, **36**, 1404.
13 H. Kikuchi, *Struct. Bonding*, 2008, **128**, 99–117.
14 I.-H. Chiang, C.-J. Long, H.-C. Lin, W.-T. Chuang, J.-J. Lee and H.-C. Lin, *ACS Appl. Mater. Interfaces*, 2014, **6**, 228–235.
15 H. Wang, Z. Zheng and D. Shen, *Liq. Cryst.*, 2012, **39**, 99–103.
16 A. Yoshizawa, *RSC Adv.*, 2013, **3**, 25475–25497.
17 M. Sato and A. Yoshizawa, *Adv. Mater.*, 2007, **19**, 4145–4148.
18 H. Iwamochi, T. Hirose, Y. Kogawa and A. Yoshizawa, *Chem. Lett.*, 2010, **39**, 170–171.
19 A. Yoshizawa, Y. Kogawa, K. Kobayashi, Y. Takanishi and J. Yamamoto, *J. Mater. Chem.*, 2009, **19**, 5759–5764.
20 M. Tanaka and A. Yoshizawa, *J. Mater. Chem. C*, 2013, **1**, 315–320.
21 C. Luo, Y. Jia, B. Sun and F. Meng, *New J. Chem.*, 2017, **41**, 3677–3686.
22 H. Kikuchi, M. Yokota, Y. Hisakado, H. Yang and T. Kajiyama, *Nat. Mater.*, 2002, **1**, 64–68.
23 Y. Chen and S.-T. Wu, *J. Appl. Polym. Sci.*, 2014, 40556.
24 L. Wang, W. He, Q. Wang, M. Yu, X. Xiao, Y. Zhang, M. Ellahi, D. Zhao, H. Yang and L. Guo, *J. Mater. Chem. C*, 2013, **1**, 6526–6531.
25 W. L. He, G. H. Pan, Z. Yang, D. Y. Zhao, G. G. Niu, W. Huang, X. T. Yuan, J. B. Guo, H. Cao and H. Yang, *Adv. Mater.*, 2009, **21**, 2050–2053.
26 B. Li, W. He, L. Wang, X. Xiao and H. Yang, *Soft Matter*, 2013, **9**, 1172–1177.
27 F. Castles, S. M. Morris, E. M. Terentjev and H. J. Coles, *Phys. Rev. Lett.*, 2010, **104**, 157801.
28 H. Wang, Z. Zheng and D. Shen, *Liq. Cryst.*, 2012, **39**, 99–103.
29 W.-Q. Yang, G.-Q. Cai, Zh. Liu, X.-Q. Wang, W. Feng, Y. Feng, D. Shen and Z. Zheng, *J. Mater. Chem. C*, 2017, **5**, 690–696.
30 K. V. Le, S. Aya, Y. Sasaki, H. Choi, F. Araoka, K. Ema, J. Mieczkowski, A. Jákli, K. Ishikawa and H. Takezoe, *J. Mater. Chem.*, 2011, **21**, 2855–2857.
31 S.-T. Hur, M.-G. Gim, H.-J. Yoo, S.-W. Choi and H. Takezoe, *Soft Matter*, 2011, **7**, 8800–8803.
32 H. C. Jeong, K. V. Le, M. J. Gim, S. T. Hur, S. W. Choi, F. Araoka, K. Ishikawa and H. Takezoe, *J. Mater. Chem.*, 2012, **22**, 4627–4630.
33 M.-J. Gim, S.-T. Hur, K.-W. Park, M. Lee, S.-W. Choi and H. Takezoe, *Chem. Commun.*, 2012, **48**, 9968–9970.
34 X. Chen, L. Wang, C. Li, J. Xiao, H. Ding, X. Liu, X. Zhang, W. He and H. Yang, *Chem. Commun.*, 2013, **49**, 10097–10099.
35 O. Jin, D. Fu, J. Wei, H. Yang and J. Guo, *RSC Adv.*, 2014, **4**, 28597–28600.
36 J. Wang, Y. Shi, K. Yang, J. Wei and J. Guo, *RSC Adv.*, 2015, **5**, 67357–67364.
37 J. L. Serrano and T. Sierra, Low Molecular Weight Calamitic Metallomesogens, in *Metallomesogens*, Wiley-VCH, Weinheim, 1996, pp. 43–123.
38 T. Seshadri and H. Haupt, *Chem. Commun.*, 1998, 735–736.
39 B. N. Veerabhadraswamy, D. S. Shankar Rao, S. Krishna Prasad and C. V. Yelamaggad, *New J. Chem.*, 2015, **39**, 2011–2027.
40 C. V. Yelamaggad, I. S. Shashikala, G. Liao, D. S. Shankar Rao, S. K. Prasad, Q. Li and A. Jákli, *Chem. Mater.*, 2006, **18**, 6100–6102.
41 C. V. Yelamaggad, V. P. Tamilenthi, A. S. Achalkumar, D. S. Shankar Rao, G. G. Nair and S. K. Prasad, *J. Mater. Chem.*, 2009, **3**, 2906–2908.

42 C.-C. Huang, Y.-H. Chen, S.-Y. Chen, Y.-Z. Sun, Z.-Y. Wu, M.-C. Yu, B.-H. Chen, I.-J. Hsu, L.-C. Wu and J.-J. Lee, *Soft Matter*, 2016, **12**, 3110–3120.

43 C.-C. Huang, Z.-Y. Wu, B.-H. Sie, W.-H. Chou, Y.-C. Huang, M.-C. Yu, B.-H. Chen, I.-J. Hsu, L.-C. Wu and J.-J. Lee, *J. Phys. Chem. B*, 2016, **120**, 12736–12754.

44 A. Boiltif and D. Louer, *J. Appl. Crystallogr.*, 2004, **37**, 724–731.

45 D. Louer and M. Louer, *J. Appl. Crystallogr.*, 1972, **5**, 271–275.

46 A. Boiltif and D. Louer, *J. Appl. Crystallogr.*, 1991, **24**, 987–993.

47 S. M. Kelly, *Helv. Chim. Acta*, 1989, **72**, 594–607.

48 H. Iwamochi and A. Yoshizawa, *Mol. Cryst. Liq. Cryst.*, 2009, **509**, 223–232.

49 M. J. Frisch, G. W. Trucks, H. B. Schlegel, G. E. Scuseria, M. A. Robb, J. R. Cheeseman, G. Scalmani, V. Barone, B. Mennucci, G. A. Petersson, H. Nakatsuji, M. Caricato, X. Li, H. P. Hratchian, A. F. Izmaylov, J. Bloino, G. Zheng, J. L. Sonnenberg, M. Hada, M. Ehara, K. Toyota, R. Fukuda, J. Hasegawa, M. Ishida, T. Nakajima, Y. Honda, O. Kitao, H. Nakai, T. Vreven, J. A. Montgomery Jr., J. E. Peralta, F. Ogliaro, M. Bearpark, J. J. Heyd, E. Brothers, K. N. Kudin, V. N. Staroverov, R. Kobayashi, J. Normand, K. Raghavachari, A. Rendell, J. C. Burant, S. S. Iyengar, J. Tomasi, M. Cossi, N. Rega, J. M. Millam, M. Klene, J. E. Knox, J. B. Cross, V. Bakken, C. Adamo, J. Jaramillo, R. Gomperts, R. E. Stratmann, O. Yazyev, A. J. Austin, R. Cammi, C. Pomelli, J. W. Ochterski, R. L. Martin, K. Morokuma, V. G. Zakrzewski, G. A. Voth, P. Salvador, J. J. Dannenberg, S. Dapprich, A. D. Daniels, Ö. Farkas, J. B. Foresman, J. V. Ortiz, J. Cioslowski and D. J. Fox, *Gaussian 09, Revision D.01*, Gaussian, Inc., Wallingford CT, 2009.

50 M. D. Hanwell, D. E. Curtis, D. C. Lonie, T. Vandermeersch, E. Zurek and G. R. Hutchison, *J. Cheminf.*, 2012, **4**, 17.

51 T. Yanai, D. P. Tew and N. C. Handy, *Chem. Phys. Lett.*, 2004, **393**, 51–57.

52 R. Dennington, T. Keith and J. Millam, *GaussView, Version 5*, Semichem Inc., Shawnee Mission, KS, 2009.

53 C.-C. Huang, C.-Y. Guo, W.-C. Hsieh, C.-Y. Fang, J.-F. Chiou, M.-J. Shyu, B.-H. Chen, I.-J. Hsu and J.-J. Lee, *RSC Adv.*, 2016, **6**, 110898–110910.

54 H. J. Coles and M. N. Pivnenko, *Nature*, 2005, **436**, 997–1000.

55 H. Chio, H. Higuchi and H. Kikuchi, *Appl. Phys. Lett.*, 2011, **98**, 726–733.

56 K. Kim, S. Kim, S.-Y. Jo and S.-W. Choi, *J. Inf. Disp.*, 2015, **16**, 155–160.